A MULTI-WAVELENGTH ANALYSIS OF RADAR-DARK HALO CRATERS ON THE MOON. A. D. Thaker*[1], C. D. Neish[1] , D. T. Blewett[2], and Y. C. Zheng[3]. [1]Institute of Earth & Space Exploration, The University of Western Ontario, London, Ontario, Canada; [2]JHU/APL, Laurel, MD, USA; [3]National Astronomical Observatories, Chinese Academy of Sciences, Beijing 100101, China. Email: athaker@uwo.ca.

Introduction: Impact cratering is a ubiquitous geological process in our solar system. It has played a significant role in shaping the landscape of many planetary bodies, including the Moon. A better understanding of impact cratering can help us to demystify the geological history and evolution of our solar system. This study focuses on a type of lunar impact craters with a distinctive ring-shaped structure surrounding them. This 'ring' exhibits unusually low radar return and circular polarization ratios (CPR); as a result, such craters are known as 'radar-dark halo craters' [1, 2]. While early work suggested that these haloes represent an ejecta layer depleted in decimeter- to meter-sized blocks [2, 3], additional data is needed to support this hypothesis. Compared to remote-sensing analysis at optical wavelengths, radar imaging and passive microwave radiometry are particularly well-suited for observing the physical properties of the lunar surface and near-subsurface, due to their greater penetration range [4].

In this work, we conduct a multi-wavelength analysis of radar-dark halo craters using the Microwave Radiometer (MRM) on China's *Chang'E-2* (CE-2) orbiter and other complimentary datasets, including ground-based and orbital radar images, and Diviner thermal-infrared (TIR) rock abundance data. We seek to improve our characterization of the scatterers present in the radar dark haloes, to better understand their origin.

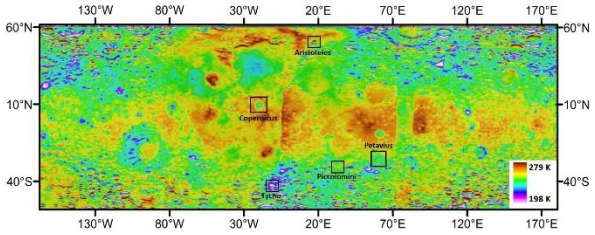

Fig 1: *Global midnight TB map derived at 3 GHz (10 cm) by the CE-2 MRM, with the black boxes highlighting locations of this study.*

Data and Method: In this study, we utilize previously calibrated MRM brightness temperature (TB) maps nomalized to lunar noon and midnight conditions at two frequencies (3 GHz and 37 GHz) by numerical statistics method [5], to determine block distribution in the near surface and the top few meters of the subsurface (Fig. 1). TB is a measure of microwave radiation emitted by the objects and is related to the physical temperature and dielectric properties of the surface and near-subsurface materials [6].

Additionally, we use P-band (70 cm) and S-band (12.6 cm) Earth-based radar data from the Arecibo Observatory and S-band data from the Miniature Radio Frequency (Mini-RF) radar on NASA's *Lunar Reconnaissance Orbiter* (LRO) [7, 8]. The radar data help us to infer the block distribution in the top few meters of the lunar regolith. Finally, we compare the TB maps with rock abundance (RA) data from LRO's Diviner TIR radiometer [9] to characterize the number of meter-sized boulders on the surface.

Using the ArcMap software package, we mapped out the boundaries of the dark haloes and continuous ejecta blankets around the craters using Arecibo P-band radar images. Then we extracted the CPR, RA and TB values from the two regions to characterize their surface and subsurface properties.

Observation: The P-band CPR images of Aristoteles (diameter D=87 km) and Copernicus (D=93 km) craters show a radar-bright continuous ejecta blanket with CPR and RA values that are higher than their surroundings (Fig. 2). This indicates increased roughness at the wavelength scale on the surface and/or in the near subsurface (Table 1).

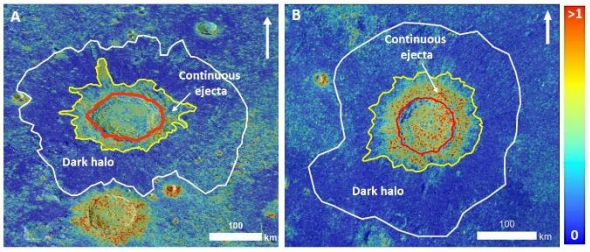

Fig 2: Arecibo *P-band CPR images of (A) Aristoteles and (B) Copernicus craters showing the dark halo.*

Beyond the continuous ejecta in both craters is a dark halo with uneven margins superposed by several small impacts. This dark halo extends out to ~1.5 times crater radii for Aristoteles and ~1 time crater radii for Copernicus. It has much lower average CPR and RA values in comparison to the continuous ejecta (Table 2).

Crater	Earth-based P-band CPR	TB at 3 GHz (K)	TB at 37 GHz (K)	Rock abundance
Aristoteles	0.6 ± 0.2	229 ± 1	212 ± 2	8 ± 14 %
Tycho	1.1 ± 0.3	224 ± 1	208 ± 1	23 ± 17%
Copernicus	0.4 ± 0.2	229 ± 0.8	213 ± 1	5 ± 6 %
Piccolomini	0.4 ± 0.1	228 ± 0.7	215 ± 1	3 ± 1 %

Table 1: *CPR, normalized midnight TB and RA values for the continuous ejecta blanket of each crater*.

Crater	Earth-based P-band CPR	TB at 3 GHz (K)	TB at 37 GHz (K)	Rock abundance
Aristoteles	0.3 ± 0.2	230 ± 1	215 ± 1	2 ± 7 %
Tycho	0.4 ± 0.1	226 ± 2	211 ± 2	3 ± 1%
Copernicus	0.1 ± 0.1	231 ± 0.5	217 ± 1	2 ± 1 %
Piccolomini	0.3 ± 0.1	228 ± 1	213 ± 1	3 ± 1 %

Table 2: *CPR, normalized midnight TB and RA values for the dark halo/discontinuous ejecta of each crater.*

The TB maps for lunar midnight at 3 and 37 GHz show marginally warmer temperatures for the dark halo compared to the continuous ejecta blanket for both craters (Fig. 3). Additionally, the TB values are higher for the 3 GHz band which represents microwave emissions from a greater depth (Table 1 and 2).

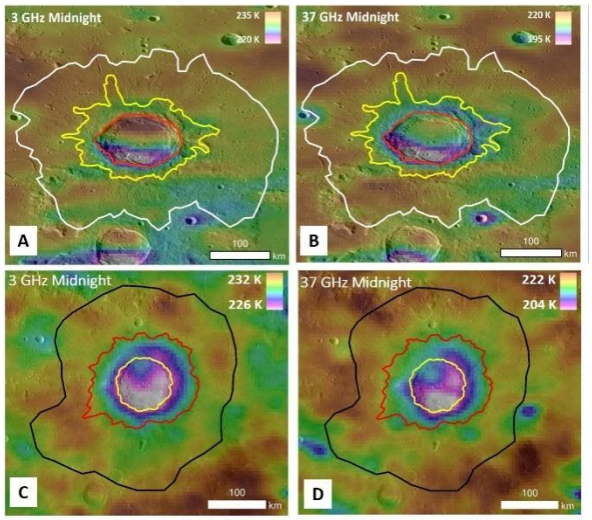

Fig 3: *Midnight TB maps at 3 and 37 GHz for (A-B) Aristoteles crater and (C-D) Copernicus crater.*

We also examined craters Tycho (D=86 km) and Piccolomini (D=88 km), which are similar in size but have no obvious halo. Similar to the radar-dark halo craters, Tycho and Piccolomini exhibit a radar-bright continuous ejecta blanket surrounding their rims (Fig. 4a); however, beyond these deposits there is no substantial difference in the average CPR or RA values compared to the surrounding terrain. Interestingly, the midnight TB data (for 3 and 37 GHz) do not show any substantially different trend compared to the dark halo craters; here we observe lower TB for the continuous ejecta deposits compared to the surrounding region (Fig. 4b, Table 1 and 2).

Discussion: For Aristoteles and Copernicus, the dark halo are easily distinguishable in the P-band (70 cm) radar images compared to the Earth-based and Mini-RF S-band (12.6 cm) images. This suggests block-poor composition at greater (P-band) depth. Additionally, the low CPR and RA values combined with warmer temperatures for the dark halo indicate an escape of microwave radiation from a rock-rich layer at

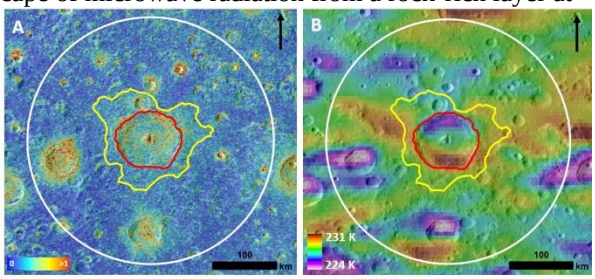

Fig 4: *(A) Earth-based P-band CPR image and (B) 3 GHz Midnight TB map of Piccolomini crater.*

depth that is overlain by a meters thick rock-poor regolith. In contrast, lower midnight TB for the continuous ejecta deposits indicate that these microwave emissions are being suppressed by a rock-rich layer in the upper part of the lunar subsurface. Additionally, we observe that for younger craters (i.e., Copernicus and Tycho) there is a distinct difference between the TB for continuous and discontinuous ejecta. However, in the case of Aristoteles and Piccolomini, which are of Eratosthenian (3.2-1.1 BY) and Upper Imbrian (3.8-3.2 BY) ages respectively, the TB values for the dark halo and continuous ejecta deposits are essentially the same. This suggests that the geological age of the craters may be one of the factors affecting the appearance of the dark haloes.

Future work: Our current work involves observations of larger (D>80 km) radar dark-halo craters and comparable non-radar-dark halo craters. In the future, we plan to expand this work to include smaller radar-dark halo craters, to determine whether crater size is an important factor in their *CPR* appearance. Additionally, we plan to include new datasets such as the FeO and TiO_2 content of the regolith (to test whether ilmenite is a factor affecting these dark haloes) and the Diviner H-parameter maps (to help us understand the properties of the top few centimeters of the lunar regolith). This work will provide insight into the mechanism responsible for the formation of these dark haloes and will expand our understanding of ejecta degradation over time.

References: [1] Ghent R. R. et al. (2005) *JGR, 110*. [2] Thomson T. W. (1974) *Moon, 10*, 51-85. [3] Ghent R. R. et al. (2010) *Icarus, 209*, 818-835. [4] Wei G. et al. (2019) *JGR Pl., 124*, 1433-1450. [5] Zheng Y. C. et al. (2019) *Icarus, 319*, 627-644. [6] Wang Z. Z. et al. (2010) *Sci. China Earth Sci., 53*, 1392-1406. [7] Campbell B. A. et al. (2007) *IEEE Trans. Geosci. Remote Sens, 45*, 4032-4042. [8] Cahill J. T. et al. (2014) *Icarus, 243*, 173-190. [9] Bandfield J. L. et al. (2011) *JGR., 116*.